ChemPubSoc Europe

DOI: 10.1002/open.201900335

Open Access
ChemistryOPEN
Full Papers

Electrons and Hydroxyl Radicals Synergistically Boost the Catalytic Hydrogen Evolution from Ammonia Borane over Single Nickel Phosphides under Visible Light Irradiation

Jin Song,[a, b] Xiaojun Gu,*[a] and Hao Zhang[a]

From the perspective of tailoring the reaction pathways of photogenerated charge carriers and intermediates to remarkably enhance the solar-to-hydrogen energy conversion efficiency, we synthesized the three low-cost semiconducting nickel phosphides Ni_2P, $Ni_{12}P_5$ and Ni_3P, which singly catalyzed the hydrogen evolution from ammonia borane (NH_3BH_3) in the alkaline aqueous solution under visible light irradiation at 298 K. The systematic investigations showed that all the catalysts had higher activities under visible light irradiation than in the dark and Ni_2P had the highest photocatalytic activity with the initial turnover frequency (TOF) value of 82.7 min^{-1}, which exceeded the values of reported metal phosphides at 298 K. The enhanced activities of nickel phosphides were attributed to the visible-light-driven synergistic effect of photogenerated electrons (e^-) and hydroxyl radicals ($^{\bullet}OH$), which came from the oxidation of hydroxide anions by photogenerated holes. This was verified by the fluorescent spectra and the capture experiments of photogenerated electrons and holes as well as hydroxyl radicals in the catalytic hydrogen evolution process.

1. Introduction

In consideration of the global environment problems, hydrogen energy has become a promising alternative to fossil fuels.[1,2] The efficient storage and release of hydrogen are main barriers during developing the hydrogen economy based on fuel cells.[3,4] Ammonia borane (NH_3BH_3) with low toxicity and high hydrogen content (19.6 wt%) is an excellent chemical hydrogen storage material.[5–7] Up to now, a variety of catalysts based on non-noble metals such as Ni and Co have been explored for the hydrogen evolution from NH_3BH_3 ($NH_3BH_3 + 2H_2O \rightarrow NH_4BO_2 + 3H_2$), which is a thermodynamics-controlled process.[8–18] However, their activities still remain low compared with the noble metal catalysts.[19–27] Thus, it is highly desirable to explore new catalytic systems using low-cost and efficient catalysts for hydrogen evolution.

Compared with the thermocatalysis, the visible-light-driven photocatalysis is considered as a friendly route for solar-to-chemical energy conversion.[28–30] Importantly, the photogenerated charge carriers in semiconductors can promote many redox reactions including hydrogen evolution from small molecules such as water.[31,32] For photocatalytic splitting of NH_3BH_3, the key is to explore low-cost catalytically active semiconductors. It has been shown that non-precious metal phosphides composed of P and earth abundant metals such as Ni have been used in water splitting as cocatalysts in photocatalysis and catalysts in electrocatalysis.[33,34] However, no attention has been paid to using these metal phosphides as photocatalysts without photosensitizers or photogenerated electron acceptors such as metal nanoparticles probably due to that they have narrow band gaps and thus have no enough redox potential to directly split water.[35] Different from the water splitting with non-spontaneous characteristics, NH_3BH_3, which has weak B–N (~117 $kJ \cdot mol^{-1}$) and B–H (~430 $kJ \cdot mol^{-1}$) bonds,[25,36] is relatively easy to split though the catalytic reaction. In addition, photogenerated charge carriers such as electrons and highly active groups such as hydroxyl radicals, which are often used to promote chemical reactions, can benefit the cleavage of B–H and B–N bonds in the photocatalytic splitting of NH_3BH_3. Bearing these aspects in mind, we considered that if semiconducting metal phosphides such as Ni_xP_y are directly used as catalysts under visible light irradiation, the efficiency of hydrogen evolution from NH_3BH_3 will be enhanced through the synergistic effect of photogenerated electrons and hydroxyl radicals.

Herein, we reported a series of low-cost metal phosphides Ni_2P, $Ni_{12}P_5$ and Ni_3P with different structures, which were for the first time used as single catalysts for hydrogen evolution from NH_3BH_3 in the alkaline aqueous solution under visible light irradiation at 298 K. Compared with the activities of all the catalysts in the dark, their visible-light-driven activities were enhanced and Ni_2P had the highest activity. Moreover, the

[a] J. Song, Prof. X. Gu, H. Zhang
Inner Mongolia Key Laboratory of Coal Chemistry
School of Chemistry and Chemical Engineering
Inner Mongolia University
Hohhot 010021, Inner Mongolia, China.
E-mail: xiaojun.gu@yahoo.com
[b] J. Song
Academician Expert Workstation of Ecological Governance and Green Development of Bayan Nur
Department of Ecology and Resource Engineering
College of Hetao
Bayan Nur 015000, Inner Mongolia, China.

Supporting information for this article is available on the WWW under https://doi.org/10.1002/open.201900335

photocatalytic hydrogen evolution mechanism was also discussed on the basis of the related experiments.

2. Results and Discussion

2.1. Synthesis Strategy

Visible-light-responsive materials with low cost were selected to catalyze hydrogen evolution from NH_3BH_3 since they can harvest visible light and then produce separated charge carriers including holes and electrons, which can promote the catalytic reaction.[37] Among the catalytically active species, nickel phosphides were selected as photocatalysts on the basis of three considerations. Firstly, nickel phosphides are active components for catalytic hydrogen evolution from NH_3BH_3, but their activities are still low. Secondly, the photogenerated charge carriers induced by the visible light might benefit the enhanced catalytic reaction rate of nickel phosphides. Thirdly, three nickel phosphides Ni_2P, $Ni_{12}P_5$ and Ni_3P with different structures, where there are different electron transfer characteristics from Ni to P,[38,39] provided us a chance to systematically study the photocatalytic chemistry of metal phosphides. Since OH^- ions in the aqueous solution are easily oxidized by photogenerated holes from semiconductors to form highly reactive hydroxyl radicals.[40] The inorganic base NaOH was selected as the resource of hydroxyl radicals, which were beneficial for the cleavage of B–N bonds in NH_3BH_3. Once the holes were consumed by OH^- ions, the remaining photogenerated electrons could efficiently participate in the splitting of NH_3BH_3. In the light of the above contents, the visible-light-driven synergistic effect of photogenerated electrons and hydroxyl radicals could lead to the efficient catalytic hydrogen evolution from NH_3BH_3 in the alkaline aqueous solution over the nickel phosphides with different structures (Figure 1).

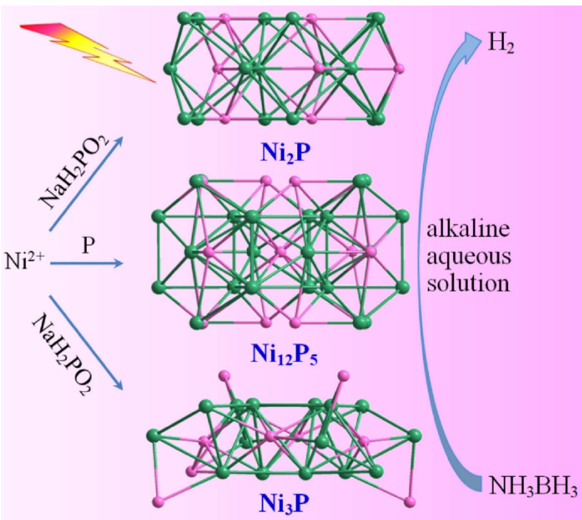

Figure 1. Schematic illustration of the catalytic hydrogen evolution procedure over single semiconducting nickel phosphides with different structures under visible light irradiation.

2.2. Structural Characterization

The crystalline phases of as-synthesized nickel phosphides were characterized using PXRD. The results showed that the pure phases of Ni_2P, $Ni_{12}P_5$ and Ni_3P were synthesized (Figure S1–S3). The surface areas of Ni_2P, $Ni_{12}P_5$ and Ni_3P were 33.2, 11.8 and 20.9 m^2/g (Figure S4–S6). The TEM images showed that the particles of Ni_2P, $Ni_{12}P_5$ and Ni_3P were in the nanoscale (Figure 2 and S7). The lattice fringes with spacing of 0.221, 0.193 and 0.180 nm corresponded to the (111) plane of Ni_2P, (240) plane of $Ni_{12}P_5$ and (222) plane of Ni_3P. The XPS investigations showed that the Ni $2p_{3/2}$ edges in the three nickel phosphides were deconvolved into three peaks (Figure 3). The peaks at 853.0, 852.7 and 852.4 eV were assigned to the positive charge $Ni^{\delta+}$ for Ni_2P, $Ni_{12}P_5$ and Ni_3P, respectively.[22,41,42] The value of δ was $\delta(Ni_2P) > \delta(Ni_{12}P_5) > \delta(Ni_3P)$. The peaks at 855.9, 856.0 and 855.9 eV were consistent to the Ni^{2+} for Ni_2P, $Ni_{12}P_5$ and Ni_3P,[43] respectively, due to the surface oxidation. The peaks at 861.3, 860.9 and 860.5 eV were assigned to the satellites of Ni $2p_{3/2}$. The spectra of Ni $2p_{1/2}$ were similar to those of Ni $2p_{3/2}$. In the P $2p_{3/2}$ spectra (Figure S8), the peaks at 128.9, 129.1 and 129.3 eV confirmed the presence of $P^{\delta-}$ for Ni_2P, $Ni_{12}P_5$ and Ni_3P,[44] respectively, indicating that there were different characteristics of charge transfer from Ni to P in the three nickel phosphides with different structures.

In the UV-vis spectra, Ni_2P, $Ni_{12}P_5$ and Ni_3P had the visible light absorption (Figure S9). The steep absorption edge suggested the electron transfer from valence band to conduction band. In order to verify the electron transfer of the nickel phosphides, we studied their transient photocurrent density under visible light irradiation ($\lambda \geq 420$ nm). The results showed that the transient photocurrent appeared in the nickel phosphides and Ni_2P had the highest photocurrent density (Figure 4a). These results also confirmed that the three nickel

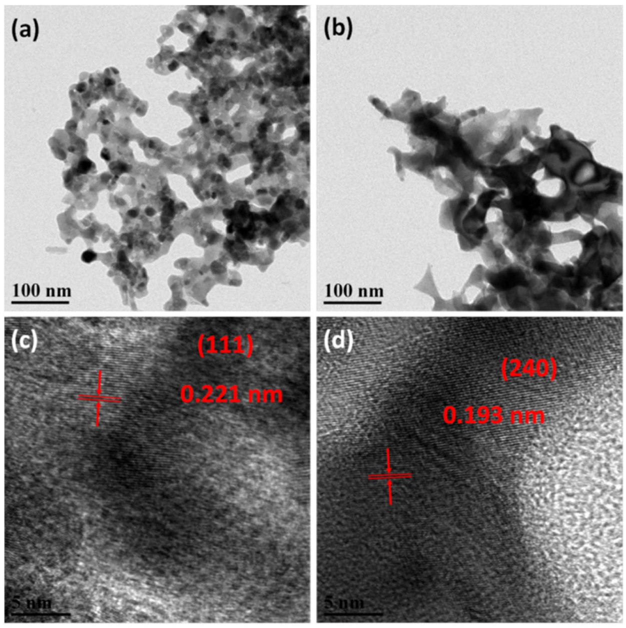

Figure 2. TEM and HRTEM mages of (a, c) Ni_2P and (b,d) $Ni_{12}P_5$.

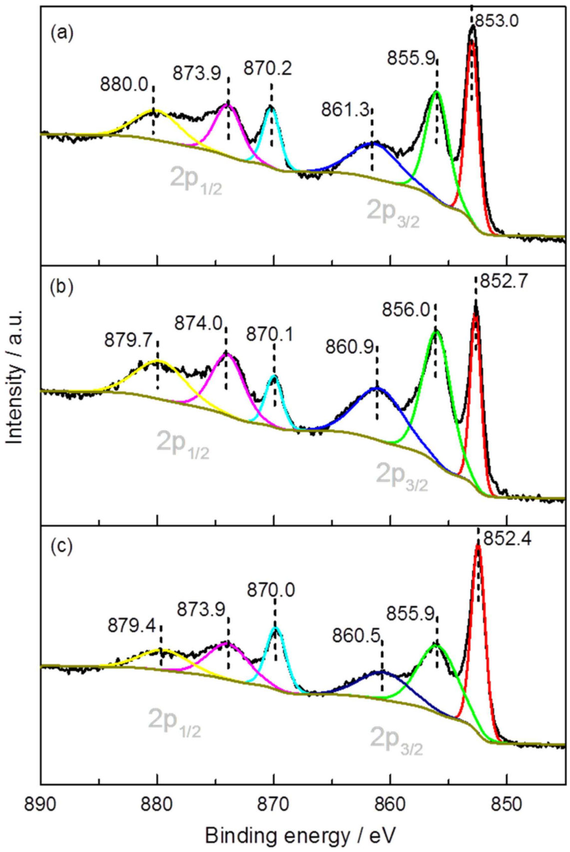

Figure 3. XPS patterns of Ni 2p for (a) Ni_2P, (b) $Ni_{12}P_5$ and (c) Ni_3P.

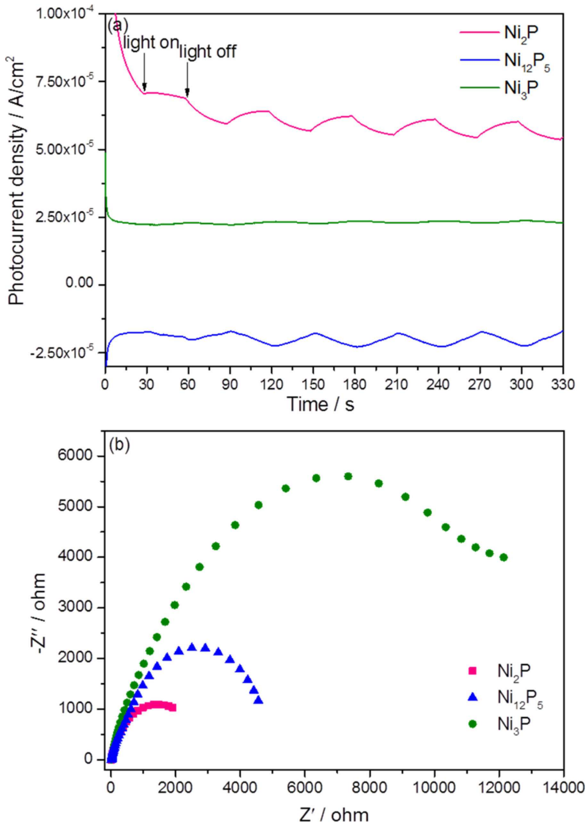

Figure 4. (a) Time versus transient photocurrent density and (b) Nyquist plots of the three nickel phosphides.

phosphides had semiconducting characteristics and Ni_2P had higher catalytic reduction ability. It should be noted that the photocurrent response of Ni_2P and Ni_3P were positive while the photocurrent response of $Ni_{12}P_5$ was negative, indicating that Ni_2P and Ni_3P were n-type semiconductors and $Ni_{12}P_5$ was p-type semiconductor.[45] These different semiconducting characteristics might lead to generating different charge carriers in the conductive process, which might further influence the photocatalytic properties of corresponding catalysts. In addition, the EIS experiments were carried out to get further insights into the hydrogen evolution ability of nickel phosphides. It was found that Ni_2P and Ni_3P had the smallest and biggest charge transfer resistance, respectively (Figure 4b), which was consistent with the corresponding transient photocurrent density.

2.3. Catalytic Performance and Mechanism

In order to investigate the effect of visible light irradiation on the catalytic performance, the hydrogen evolution from NH_3BH_3 in the alkaline aqueous solution over Ni_2P, $Ni_{12}P_5$ and Ni_3P was measured. As shown in Figure 5, the activities of three catalysts were enhanced under visible light irradiation compared with their activities in the dark. Specially, Ni_2P exhibited the highest activity with the initial turnover frequency (TOF) value of 82.7 min^{-1}, which was the highest in the values of reported metal phosphide catalysts (Table 1). The 87.5, 78.7 and 88.2% of activity enhancement of Ni_2P, $Ni_{12}P_5$ and Ni_3P was caused by the contribution of visible light irradiation comparable to the dark reaction, respectively. The different activity enhancement could be attributed to the different light absorption ability and the different charge separation efficiency with increasing the Ni/P ratio from 2 to 3 in these nickel phosphides, which might lead to the different usage efficiency of photogenerated charge carriers and hydroxyl radicals. In addition, the characteristic of electron transfer from Ni to P in the three nickel phosphides with different Ni/P ratios was different (Figure 3), which led to their different photocatalytic hydrogen evolution activities. It

Table 1. Activities of catalysts for hydrogen evolution from NH_3BH_3.

Catalyst	TOF (min^{-1})	Reference
Ni_2P	82.7	This work
$Ni_{0.8}W_{0.2}$	25.0	6
Ni	19.6	14
$Co/(CeO_x)_{0.91}/NGH$	79.5	15
$Cu_{0.72}Co_{0.18}Mo_{0.1}$	46	16
CoP	72.2	17
$Ni_{0.7}Co_{1.3}P$	58.4	18
$Pd_{74}Ni_{26}/MCN$	246.8	20
$Cu_xCo_{1-x}O$–GO	70.0	24
Co/CTF	42.3	25
Co/C_3N_4-580	93.8	37

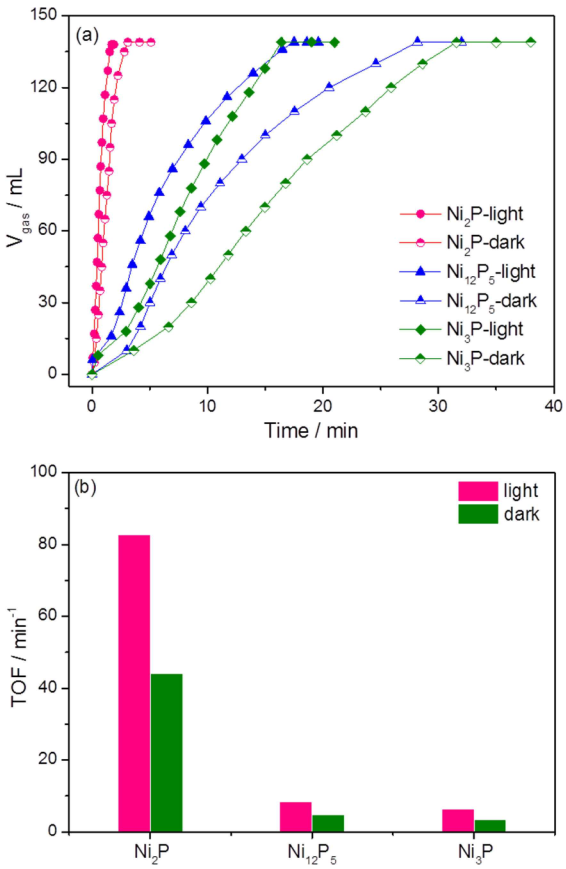

Figure 5. (a) Time versus volume of hydrogen evolution from the alkaline aqueous NH_3BH_3 over the three nickel phosphides under different conditions and (b) the initial TOF values.

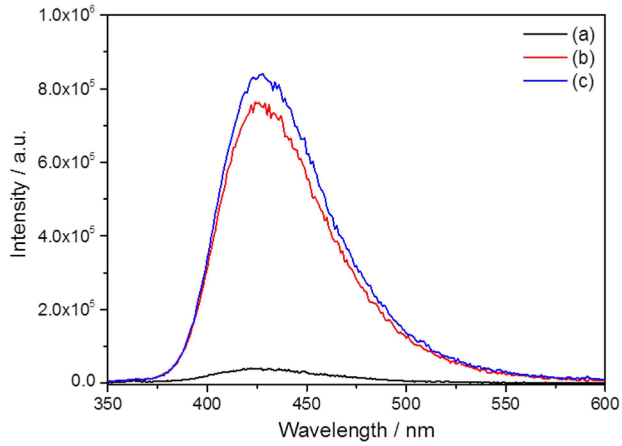

Figure 6. Fluorescent spectra of Ni_2P in (a) 10.0, (b) 30.0 and (c) 50.0 mM of alkaline aqueous solution and TA (5 mM) under visible light irradiation.

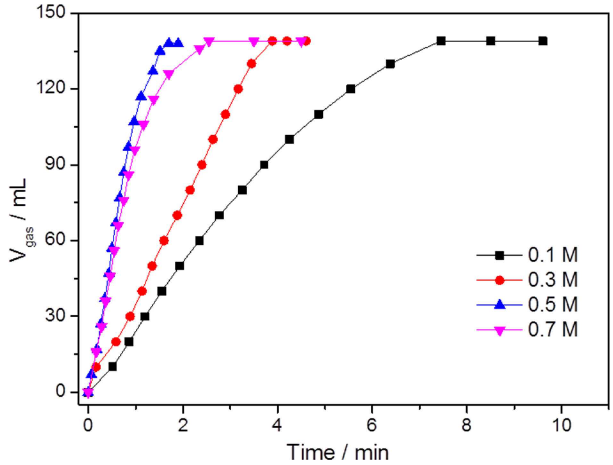

Figure 7. Time versus volume of hydrogen evolution from NH_3BH_3 in the aqueous solution with different alkaline concentrations over Ni_2P under visible light irradiation.

should be noted that the crystalline phases of three nickel phosphides were maintained after the catalytic hydrogen evolution reaction (Figure S1–S3), indicating that these photocatalysts were stable in the present alkaline environment.

The formation of radical intermediates under the light irradiation of photoactive materials in aqueous environment plays an important role in the photocatalytic reactions.[46,47] It is known that hydroxyl radicals can react with TA and generate TAOH, which emits fluorescence at around 426 nm. To investigate the effect of hydroxyl radicals, which generated in a process of oxidation of OH^- or H_2O by photogenerated holes, on the catalytic activity, we selected TA as fluorescence probe to trace the hydroxyl radicals. The results showed that the concentration of OH^- affected the amount of produced hydroxyl radicals and there was different intensity of fluorescence peaks, which appeared at about 426 nm (Figure 6). More importantly, the photocatalytic hydrogen evolution rate increased with increasing the base concentration (Figure 7). In detail, Ni_2P had the highest activity in 0.5 M of NaOH. However, its activity decreased when the alkaline concentration increased to 0.7 M. The high-concentration base induced the formation of more hydroxyl radicals, which participated in the cleavage of chemical bonds in NH_3BH_3, while the excessive hydroxyl radicals impeded the adsorption of catalytic substrates NH_3BH_3 and H_2O on the surface of catalyst. Besides, the base NaOH also acted as a catalyst promoter for the hydrolytic dehydrogenation of NH_3BH_3.[16–18] This suggested that the formation of hydroxyl radicals benefited the catalytic activity enhancement under visible light irradiation. To further make sure the existence of hydroxyl radicals, we tested the photocatalytic activity of Ni_2P, where 2-propanol was chosen as the scavenger of hydroxyl radicals. The results showed the activity decreased due to the decrease of hydroxyl radicals (Figure 8), indicating that the formation of hydroxyl radicals was a positive factor for photocatalytic hydrogen evolution from NH_3BH_3.

In the present catalytic system, the hydroxyl radicals generated through the oxidation of OH^- ions by photogenerated holes.[48,49] In order to confirm this judgment, we measured the photocatalytic activity of Ni_2P, where KI was used as capture agent of holes. The results showed that the catalytic activity decreased due to the decrease of holes (Figure 8), suggesting that the formation of holes had a positive effect on the catalytic reaction rate in the alkaline aqueous solution.

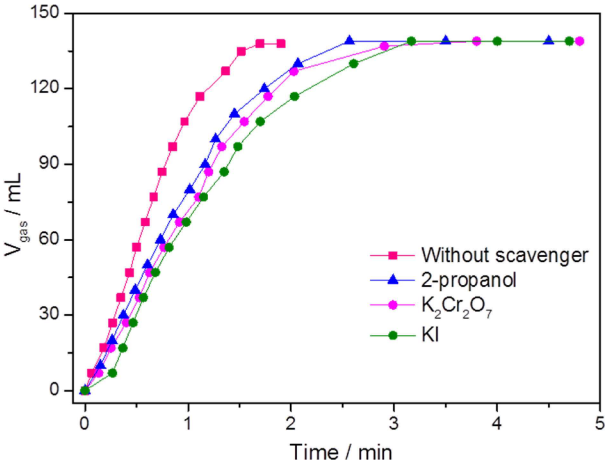

Figure 8. Time versus volume of hydrogen evolution from the alkaline aqueous NH_3BH_3 over Ni_2P without scavenger or in the presence of 2-propanol, $K_2Cr_2O_7$ and KI under visible light irradiation.

Besides the photogenerated holes, the photogenerated electrons also played an important role in the catalytic reaction.[50] To check this, $K_2Cr_2O_7$ was selected as scavenger of electrons in the catalytic process. The results showed that the photocatalytic activity decreased after the introduction of $K_2Cr_2O_7$ (Figure 8), indicating that the photocatalytic hydrogen evolution was remarkably affected by the photogenerated electrons.

In view of the above results regarding hydroxyl radicals and photogenerated charge carriers, a possible mechanism for photocatalytic hydrogen evolution from NH_3BH_3 in the alkaline aqueous solution was proposed (Figure 9). After the absorption of visible light by nickel phosphides, the photogenerated electrons and holes formed, separated and migrated to the catalyst surface. In the meantime, the hydroxyl radicals generated through the reaction between photogenerated holes and OH^- ions. For the decomposition of NH_3BH_3 for hydrogen evolution, the cleavage of B–N bonds, which form through enjoying lone pair electrons between NH_3 and BH_3 groups, should first happen. On the basis of that the hydroxyl radicals benefited the enhancement of photocatalytic hydrogen evolution from NH_3BH_3 in the experiment, it could be rationally deduced that the hydroxyl radicals attacked NH_3BH_3 to break the B–N bond and the photogenerated electrons attacked the B–H bond to generate H_2 with the assistance of water.

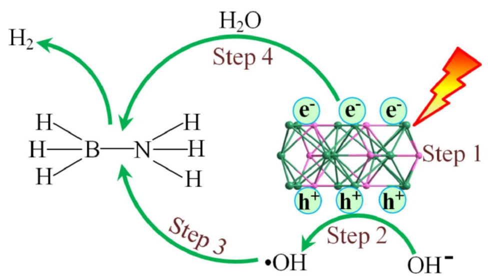

Figure 9. Possible mechanism for the hydrogen evolution from NH_3BH_3 in the alkaline aqueous solution over nickel phosphides under visible light irradiation.

To further understand the role of visible light irradiation in the activity enhancement of catalysts, the catalytic performance of Ni_2P under different light intensity was investigated. It was found that increasing the light intensity resulted in an almost linear enhancement of catalytic activity (Figure 10). These phenomena could be attributed to that more electrons and hydroxyl radicals generated from Ni_2P in the alkaline environment under high-intensity visible light irradiation, leading to that more photogenerated electrons and hydroxyl radicals were used to attack and break B–H and B–N bonds in NH_3BH_3

In the present reaction, water molecules participate in the hydrogen evolution.[5,51] In order to confirm this judgment, we used D_2O instead of H_2O to investigate the kinetic isotope effect (KIE) in the catalytic reaction over Ni_2P, $Ni_{12}P_5$ and Ni_3P. The results showed that the hydrolysis of NH_3BH_3 in D_2O had a low reaction rate compared to that in H_2O under light irradiation (Figure 11 and S10). The KIE constants were 2.9, 2.8 and 2.4 calculated according to the hydrogen evolution rate. This indicated that water molecules were involved in the hydrogen evolution from the aqueous NH_3BH_3, which was similar to the hydrogen evolution through the hydrolysis of $NaBH_4$.[52]

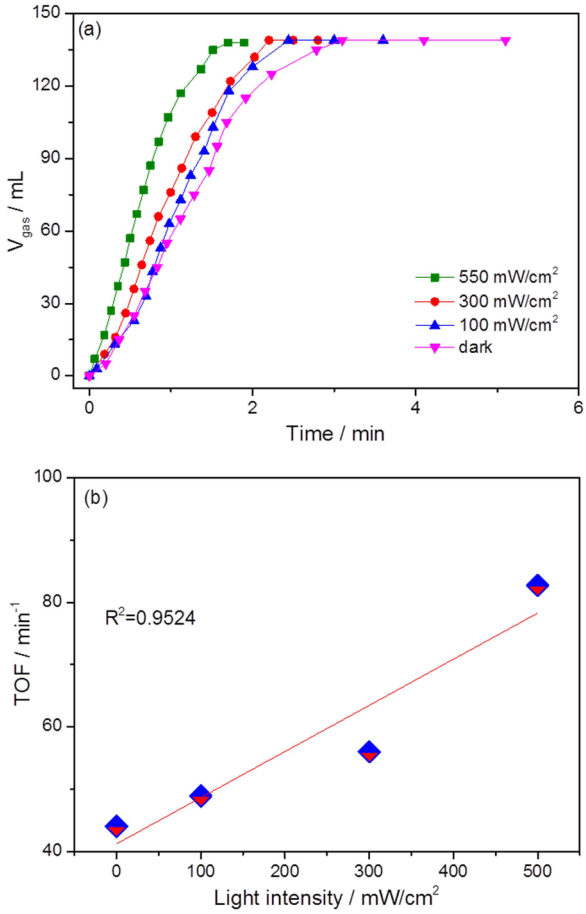

Figure 10. (a) Time versus volume of hydrogen evolution from the alkaline aqueous NH_3BH_3 over Ni_2P under visible light irradiation with different intensities and (b) the dependence of initial TOF values on the light intensity.

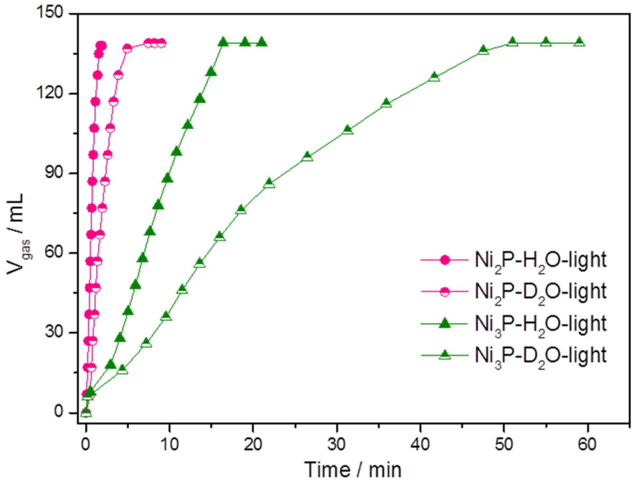

Figure 11. Time versus volume of hydrogen evolution from NH_3BH_3 in H_2O or D_2O over Ni_2P and Ni_3P under visible light irradiation.

It is known that the hydrogen evolution from aqueous NH_3BH_3 is a thermodynamics-controlled process.[53] In order to evaluate the effect of reaction temperature on the photocatalysis, we measured the photocatalytic performance of Ni_2P under the photothermal condition. The results showed that compared with the photocatalytic activity of Ni_2P at 298 K, its activity was significantly enhanced under photothermal condition and its initial TOF value was 138.3 min^{-1} (Figure S11), which was much higher than the value (82.7 min^{-1}) at room temperature.

The practical application of catalysts requires their good recycle durability. So the long-time catalytic durability test of Ni_2P under visible light irradiation was carried out at 298 K. The results showed that the catalyst had good durability and 100% of H_2 selectivity even after 20 cycles of catalysis (Figure 12a). After the catalytic cycles, the crystalline phase of Ni_2P was unchanged (Figure 12b). With increasing the number of catalytic cycles, the rate of hydrogen evolution decreased, which might be due to the agglomeration of catalyst particles after the long-time photocatalytic reaction (Figure 12c). In addition, the increase of boron species in the catalytic system might also lead to the gradual decrease of hydrogen evolution rate.[5]

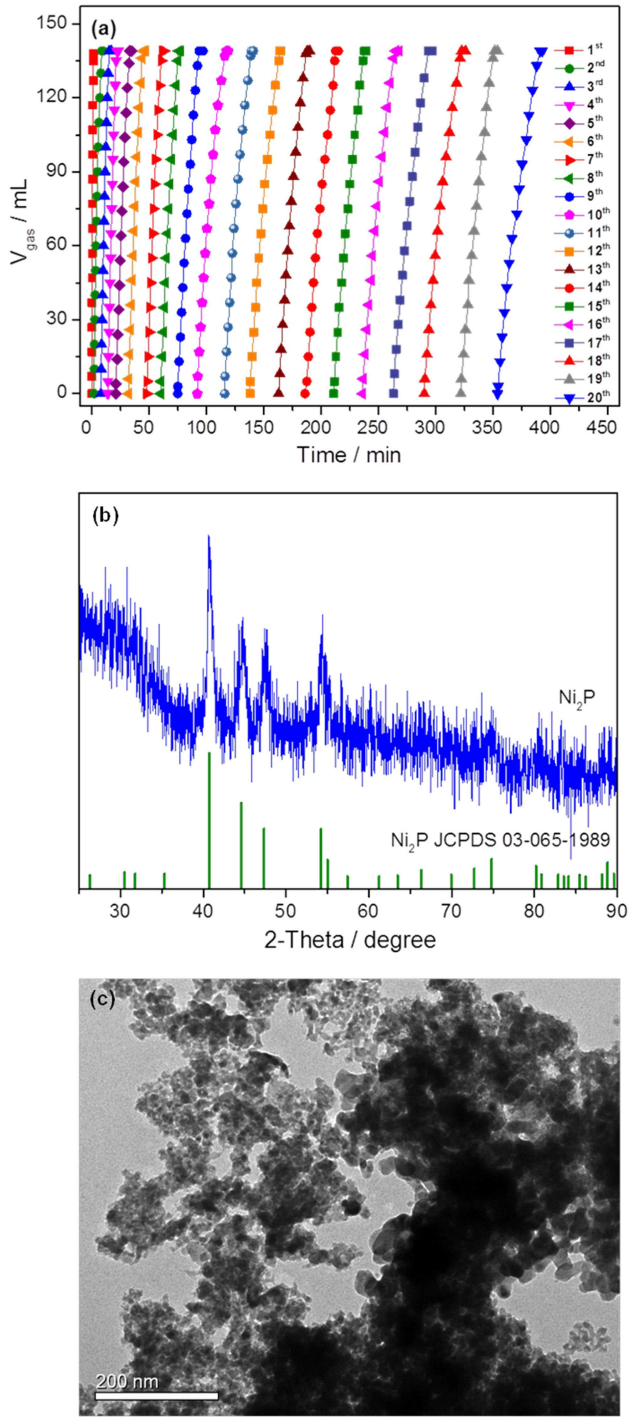

Figure 12. Durability test for the hydrogen evolution from the alkaline aqueous NH_3BH_3 over Ni_2P, (b) the PXRD pattern and (c) the TEM image of catalyst after 20 cycles of catalysis.

3. Conclusions

In summary, three semiconducting nickel phosphides Ni_2P, $Ni_{12}P_5$ and Ni_3P with different structures were synthesized. The compounds were used as single catalysts for hydrogen evolution from NH_3BH_3 under visible light irradiation. Among all the catalysts, Ni_2P had the highest room-temperature activity. In the catalytic process, the synergistic effect of photogenerated electrons and hydroxyl radicals in the alkaline aqueous condition enhanced the activities of nickel phosphides under visible light irradiation. This effect has been experimentally testified by the fluorescent spectra and the capture of photogenerated charge carriers and hydroxyl radicals as well as the related hydrogen evolution performance of the catalysts. Based on the obtained results, a new mechanism for the photocatalytic hydrogen evolution from NH_3BH_3 in the alkaline aqueous solution has been presented. This work sheds light on exploring low-cost and visible-light-responsive semiconductors with well-defined structures, which is beneficial for rationally designing new high-performance photocatalytic systems toward a greener world using clean energy.

Experimental Section

Chemicals

Nickel chloride hexahydrate ($NiCl_2\cdot 6H_2O$, Sinopharm Chemical Reagent Co. Ltd, >99%), sodium hypophosphite (NaH_2PO_2, Aladdin, 99%), trisodium citrate dihydrate ($Na_3C_6H_5O_7\cdot 2H_2O$, Sinopharm Chemical Reagent Co. Ltd, >99%), phosphorus red (P, Aladdin, 99%), sodium acetate (CH_3COONa, Sinopharm Chemical Reagent Co. Ltd, >99%), nickel acetate tetrahydrate ($Ni(CH_3COO)_2\cdot 4H_2O$, Sinopharm Chemical Reagent Co. Ltd, >99%), potassium dichromate ($K_2Cr_2O_7$, Sinopharm Chemical Reagent Co. Ltd, 99.8%), potassium hydroxide (KOH, Sinopharm Chemical Reagent Co. Ltd, >85%), potassium iodide (KI, J&K Chemical, >99%), sodium hydroxide (NaOH, Sinopharm Chemical Reagent Co. Ltd, >96%), ammonia borane (NH_3BH_3, Aldrich, 97%), terephtalic acid ($C_8H_6O_4$, TA, J&K Chemical, 99%), 2-propanol ($(CH_3)_2CHOH$, J&K Chemical, 99.9%) and deuterium oxide (D_2O, J&K Chemical, 99.8% atom D) were obtained without purification.

Synthesis and Catalytic Study

For the synthesis of Ni_2P,[22] the mixture of $NiCl_2\cdot 6H_2O$ (1.00 g), $Na_3C_6H_5O_7\cdot 2H_2O$ (0.25 g) and NaOH (2.80 g) in water (45 mL) was stirred for 1 h to give a green solid. Then, the green solid (0.25 g) and NaH_2PO_2 (1.25 g) were heated at 573 K for 2 h in an Ar atmosphere to give Ni_2P. For the synthesis of $Ni_{12}P_5$,[39] the mixture of $Ni(CH_3COO)_2\cdot 4H_2O$ (0.95 g) and phosphorus red (0.70 g) was dissolved in water (30 mL) under stirring for 20 min. Then, the mixture was hydrothermally treated at 473 K for 12 h to give $Ni_{12}P_5$. For the synthesis of Ni_3P,[54] the mixture of $NiCl_2\cdot 6H_2O$ (5.0 g), NaH_2PO_2 (24.4 g) and CH_3COONa (2.9 g) was dissolved in water (100 mL). The KOH was used to adjust the solution pH to 8.0. Then the solution was heated at 363 K for 1 h to give a black solid. Later, the black solid was calcined at 673 K for 1 h in an Ar atmosphere. Finally, the product was washed in HCl solution, water and ethanol, resulting in Ni_3P.

The catalytic reaction was performed under visible light irradiation at 298 K or in the dark at 298 K in the aqueous solution (3.0 mL) of NH_3BH_3 (1.71 mmol) and NaOH with different concentrations. The molar ratio of Ni_xP_y/NH_3BH_3 was 0.03 in the catalytic reaction. The reaction temperature was kept at 298 K through the cooling water circulating pump.

Catalyst Characterization

The transmission electron microscopy (TEM, JEM-2010) was applied to confirm the morphologies of samples. The UV-vis, the fluorescent and the surface area measurements were conducted on a Shimadzu UV-3600 spectrometer, a FLS920 spectrometer and an Autosorb-iQ2-MP adsorption equipment, respectively. Powder X-ray diffraction (PXRD) and X-ray photoelectron spectroscopy (XPS) were performed using an X-ray diffractmeter (Panalytical X-Pert) and an instrument (ESCALAB250, Thermo VG Corp.). An electrochemical station (PGSTAT302N, Switzerland) was used to measure the transient photocurrent and electrochemical impedance spectroscopy (EIS) in the 1.0 M of Na_2SO_4 aqueous solution. An Ag/AgCl electrode, an indium tin oxide (ITO) glass covered with metal phosphides and a Pt plate were selected as the reference electrode, the working electrode and the counter electrode, respectively.

Calculation Method

The initial TOF value was calculated at the NH_3BH_3 conversion of 72%. The calculation was shown as follow:

$$TOF = \frac{3n_{NH3BH3}}{n_{catalyst}t} \times 72\%$$

In the equation, n_{NH3BH3} is the molar amount of NH_3BH_3 at its conversion of 72%, $n_{catalyst}$ is the total molar amount of nickel phosphide and t is the time at the NH_3BH_3 conversion of 72%.

Acknowledgements

The authors gratefully acknowledge the financial support from the National Natural Science Foundation of China (21761025), the Program for New Century Excellent Talents in University of the Ministry of Education of China (NCET-13-0846) and the Pilot Support Project for Ecological Conservation and Restoration of Landscape, Forest, Lake and Grassland in Lake Ulansuhai (2019HYYSZX).

Conflict of Interest

The authors declare no conflict of interest.

Keywords: synergistic effect · ammonia borane · hydrogen evolution · catalysts

[1] A. Boddien, D. Mellmann, F. Gärtner, R. Jackstell, H. Junge, P. J. Dyson, G. Laurenczy, R. Ludwig, M. Beller, *Science* **2011**, *333*, 1733–1736.
[2] X. Gu, Z.-H. Lu, H.-L. Jiang, T. Akita, Q. Xu, *J. Am. Chem. Soc.* **2011**, *133*, 11822–11825.
[3] X. Xu, Y. Chen, W. Zhou, Z. Zhu, C. Su, M. Liu, Z. Shao, *Adv. Mater.* **2016**, *28*, 6442–6448.
[4] J.-M. Yan, Z.-L. Wang, L. Gu, S.-J. Li, H.-L. Wang, W.-T. Zheng, Q. Jiang, *Adv. Energy Mater.* **2015**, *5*, 1500107.
[5] Q.-L. Zhu, Q. Xu, *Energy Environ. Sci.* **2015**, *8*, 478–512.
[6] K. Yang, Q. Yao, W. Huang, X. Chen, Z.-H. Lu, *Int. J. Hydrogen Energy* **2017**, *42*, 6840–6850.
[7] Z. Tang, H. Chen, X. Chen, L. Wu, X. Yu, *J. Am. Chem. Soc.* **2012**, *134*, 5464–5467.
[8] D. Sun, V. Mazumder, Ö. Metin, S. Sun, *ACS Nano* **2011**, *5*, 6458–6464.
[9] K. Guo, H. Li, Z. Yu, *ACS Appl. Mater. Interfaces* **2018**, *10*, 517–525.
[10] Q.-L. Zhu, J. Li, Q. Xu, *J. Am. Chem. Soc. Rev.* **2013**, *135*, 10210–10213.
[11] F. Qiu, Y. Dai, L. Li, C. Xu, Y. Huang, C. Chen, Y. Wang, L. Jiao, H. Yuan, *Int. J. Hydrogen Energy* **2014**, *39*, 436–441.
[12] K. Aranishi, Q.-L. Zhu, Q. Xu, *ChemCatChem* **2014**, *6*, 1375–1379.
[13] X. Feng, X.-M. Chen, P. Qiu, D. Wu, E. J. M. Hamilton, J. Zhang, X. Chen, *Int. J. Hydrogen Energy*, **2018**, *43*, 20875–20881.
[14] C.-Y. Cao, C.-Q. Chen, W. Li, W.-G. Song, W. Cai, *ChemSusChem* **2010**, *3*, 1241–1244.
[15] Y. Men, J. Su, C. Huang, L. Liang, P. Cai, G. Cheng, W. Luo, *Chin. Chem. Lett.* **2018**, *29*, 1671–1674.
[16] Q. Yao, K. Yang, X. Hong, X. Chen, Z. Lu, *Catal. Sci. Technol.* **2018**, *8*, 870–877.
[17] Z.-C. Fu, Y. Xu, S. L.-F. Chan, W.-W. Wang, F. Li, F. Liang, Y. Chen, Z.-S. Lin, W.-F. Fu, C.-M. Che, *Chem. Commun.* **2017**, *53*, 705–708.
[18] C.-C. Hou, Q. Li, S. C.-J. Wang, C.-Y. Peng, Q.-Q. Chen, H.-F. Ye, W.-F. Fu, C.-M. Che, N. López, Y. Chen, *Energy Environ. Sci.* **2017**, *10*, 1770–1776.
[19] T. Karaca, M. Sevim, Ö. Metin, *ChemCatChem* **2017**, *9*, 4185–4190.
[20] W. Wang, Z.-H. Lu, Y. Luo, A. Zou, Q. Yao, X. Chen, *ChemCatChem* **2018**, *10*, 1620–1626.

[21] Q. Yao, W. Shi, G. Feng, Z.-H. Lu, X. Zhang, D. Tao, D. Kong, X. Chen, *J. Power Sources* **2014**, *257*, 293–299.
[22] C.-Y. Peng, L. Kang, S. Cao, Y. Chen, Z.-S. Lin, W.-F. Fu, *Angew. Chem.* **2015**, *127*, 15951–15955; *Angew. Chem. Int. Ed.* **2015**, *54*, 15725–15729.
[23] Q. Yao, Z.-H. Lu, W. Huang, X. Chen, J. Zhu, *J. Mater. Chem. A* **2016**, *4*, 8579–8583.
[24] K. Feng, J. Zhong, B. Zhao, H. Zhang, L. Xu, X. Sun, S.-T. Lee, *Angew. Chem.* **2016**, *128*, 12129–12133; *Angew. Chem. Int. Ed.* **2016**, *55*, 11950–11954.
[25] Z. Li, T. He, L. Liu, W. Chen, M. Zhang, G. Wu, P. Chen, *Chem. Sci.* **2017**, *8*, 781–788.
[26] L. Wen, J. Su, X. Wu, P. Cai, W. Luo, G. Cheng, *Int. J. Hydrogen Energy* **2014**, *39*, 17129–17135.
[27] L. Yang, J. Su, W. Luo, G. Cheng, *Int. J. Hydrogen Energy* **2014**, *39*, 3360–3370.
[28] J. Ran, J. Zhang, J. Yu, M. Jaroniec, S. Z. Qiao, *Chem. Soc. Rev.* **2014**, *43*, 7787–7812.
[29] Y.-J. Yuan, Z.-T. Yu, D.-Q. Chen, Z.-G. Zou, *Chem. Soc. Rev.* **2017**, *46*, 603–631.
[30] L.-Z. Wu, B. Chen, Z.-J. Li, C.-H. Tung, *Acc. Chem. Res.* **2014**, *47*, 2177–2185.
[31] Y. He, D. Wang, *Chem* **2018**, *4*, 405–408.
[32] R. Asahi, T. Morikawa, H. Irie, T. Ohwaki, *Chem. Rev.* **2014**, *114*, 9824–9852.
[33] Z. Sun, H. Zheng, J. Li, P. Du, *Energy Environ. Sci.* **2015**, *8*, 2668–2676.
[34] C. Tang, R. Zhang, W. Lu, Z. Wang, D. Liu, S. Hao, G. Du, A. M. Asiri, X. Sun, *Angew. Chem.* **2017**, *129*, 860–864; *Angew. Chem. Int. Ed.* **2017**, *56*, 842–846.
[35] M. Sharon, G. Tamizhmani, C. Levy-Clement, J. Rioux, *Sol. Cells* **1989**, *26*, 303–312.
[36] P. R. Rablen, *J. Am. Chem. Soc.* **1997**, *119*, 8350–8360.
[37] H. Zhang, X. Gu, J. Song, N. Fan, H. Su, *ACS Appl. Mater. Interfaces* **2017**, *9*, 32767–32774.
[38] Y. Pan, Y. Liu, J. Zhao, K. Yang, J. Liang, D. Liu, W. Hu, D. Liu, Y. Liu, C. Liu, *J. Mater. Chem. A* **2015**, *3*, 1656–1665.
[39] Y. Deng, Y. Zhou, Y. Yao, J. Wang, *J. New. Chem.* **2013**, *37*, 4083–4088.
[40] T. Y. Wei, C. C. Wan, *Ind. Eng. Chem. Res.* **1991**, *30*, 1293–1300.
[41] Z. Sun, M. Zhu, M. Fujitsuka, A. Wang, C. Shi, T. Majima, *ACS Appl. Mater. Interfaces* **2017**, *9*, 30583–30590.
[42] Y. Chen, C. Li, J. Zhou, S. Zhang, D. Rao, S. He, M. Wei, D. G. Evans, X. Duan, *ACS Catal.* **2015**, *5*, 5756–5765.
[43] Z. Huang, Z. Chen, Z. Chen, C. Lv, H. Meng, C. Zhang, *ACS Nano* **2014**, *8*, 8121–8129.
[44] A. Indra, A. Acharjya, P. W. Menezes, C. Merschjann, D. Hollmann, M. Schwarze, M. Aktas, A. Friedrich, S. Lochbrunner, A. Thomas, M. Driess, *Angew. Chem.* **2017**, *129*, 1675–1679; *Angew. Chem. Int. Ed.* **2017**, *56*, 1653–1657.
[45] L. Xiong, S. Huang, X. Yang, M. Qiu, Z. Chen, Y. Yu, *Electrochim. Acta* **2011**, *56*, 2735–2739.
[46] M. Pelaez, N. T. Nolan, S. C. Pillai, M. K. Seery, P. Falaras, A. G. Kontos, P. S. M. Dunlop, J. W. J. Hamilton, J. A. Byrne, K. O'Shea, M. H. Entezari, D. D. Dionysiou, *Appl. Catal. B* **2012**, *125*, 331–349.
[47] F. Dong, Z. Zhao, Y. Sun, Y. Zhang, S. Yan, Z. Wu, *Environ. Sci. Technol.* **2015**, *49*, 12432–12440.
[48] I. K. Konstantinou, T. A. Albanis, *Appl. Catal. B* **2004**, *49*, 1–14.
[49] K. Mori, P. Verma, R. Hayashi, K. Fuku, H. Yamashita, *Chem. Eur. J.* **2015**, *21*, 11885–11893.
[50] S. Jo, P. Verma, Y. Kuwahara, K. Mori, W. Choi, H. Yamashita, *J. Mater. Chem. A* **2017**, *5*, 21883–21892.
[51] H. Ma, C. Na, *ACS Catal.* **2015**, *5*, 1726–1735.
[52] G. Guella, C. Zanchetta, B. Patton, A. Miotello, *J. Phys. Chem. B* **2006**, *110*, 17024–17033.
[53] W.-W. Zhan, Q.-L. Zhu, Q. Xu, *ACS Catal.* **2016**, *6*, 6892–6905.
[54] L. Jin, H. Xia, Z. Huang, C. Lv, J. Wang, M. G. Humphrey, C. Zhang, *J. Mater. Chem. A* **2016**, *4*, 10925–10932.

Manuscript received: November 12, 2019
Revised manuscript received: February 2, 2020